# Nonisothermal Crystallization Behaviors of Silk-Fibroin-Fiber-Reinforced Poly(ε-caprolactone) Biocomposites

**Xiuying Qiao,[1] Wei Li,[1] Kang Sun,[1] Shi Xu,[2] Xiaodong Chen[3]**

[1]*State Key Laboratory of Metal Matrix Composites, Shanghai Jiao Tong University, Shanghai 200240, China*
[2]*Instrumental Analysis Center, Shanghai Jiao Tong University, Shanghai 200240, China*
[3]*Shanghai Sunny New Technology Development Company, Limited, Shanghai 201108, China*

Received 28 March 2008; accepted 7 August 2008
DOI 10.1002/app.29232
Published online 5 December 2008 in Wiley InterScience (www.interscience.wiley.com).

**ABSTRACT:** With differential scanning calorimetry measurements, the nonisothermal crystallization of biocomposites of poly(ε-caprolactone) (PCL) reinforced with silk fibroin fiber (SF) was investigated. With the gradual addition of SF, the strengthening of the heterogeneous nucleation reagent effect of SF led to the acceleration of PCL crystallization, and secondary crystallization occurred and became more remarkable with increases in the cooling rate and SF content. Moreover, with the introduction of SF and an increase in the cooling rate, the nucleation and growth mode of the PCL crystalline phase was slightly changed. Because of the confinement of the fiber network structure, the crystallite size of PCL was reduced, the crystallization exothermicity of PCL decreased, and the crystallization activation energy of PCL increased. © 2008 Wiley Periodicals, Inc. J Appl Polym Sci 111: 2908–2916, 2009

**Key words:** biopolymers; composites; crystallization; differential scanning calorimetry (DSC); fibers

## INTRODUCTION

Poly(ε-caprolactone) (PCL) as a biodegradable aliphatic polyester has attracted great attention because of its widespread applications in pharmaceutical controlled-release systems, implanted polymer devices, and biodegradable packaging materials.[1,2] However, the relatively low strength and modulus of PCL have caused some limits to its applications, especially for bone substitutes. For improving the mechanical properties and biodegradability of some biodegradable polymer materials, biodegradable natural fibers with high strength, high toughness, and good biocompatibility are attractive candidates for utilization.[3–7] Several studies have demonstrated that with the introduction of some natural fibers such as abaca,[6] chitin,[8] lignin,[9] and cellulose,[10] the flexural strength, Young's modulus, and yield stress of PCL can be remarkably enhanced.

As a kind of natural fiber, silk fiber (*Bombyx mori*), spun from silkworm cocoons, mainly consists of two protein-based components, inner fibroin filaments (75 wt %) and outer sericin (25 wt %); the former is a real fibrous component with high crystallinity and good alignment along the fiber.[11] Before silk fiber is used, a degumming process is usually performed to remove the sericin component to achieve better mechanical properties.[12,13] In recent years, silk fiber has been paid more and more attention by researchers because of its excellent mechanical properties, outstanding biocompatibility characteristics with living tissues, and great potential for biotechnological and biomedical applications.[14,15]

The investigation of the crystallization behavior of polymer materials, especially the nonisothermal crystallization behavior, is very significant for both theory and practice because crystallization usually occurs under nonisothermal conditions during production and the physical and mechanical properties of the products are intimately related to the degree of crystallization and the morphology and structures of the crystals. Differential scanning calorimetry is an effective medium for probing nonisothermal crystallization behavior. Some nonisothermal crystallization kinetic methods are widely used for polymer systems,[16–19] most of which are derived from the Avrami equation.[20,21] It has been reported that the addition of a small amount of multiwalled carbon nanotubes to PCL causes a change in the mechanism of nucleation and crystal growth of PCL crystallites.[22] As for PCL/$SiO_2$ hybrid materials, different compositions induce various structures and microphase-scale separation, and this in turn influences the crystallization behavior and mechanism of PCL in these composites correspondingly.[23]

Although some research has been focused on the crystallization behaviors of some fiber-reinforced PCL composites,[22–25] the nonisothermal crystallization behaviors of silk-fibroin-fiber-reinforced poly

*Correspondence to:* X. Qiao (xyqiao@sjtu.edu.cn).

(ε-caprolactone) (SF/PCL) composites have not been reported yet. In this study, after degumming treatments, the obtained silk fibroin fiber (SF) was used to prepare novel reinforced PCL biocomposites, and their nonisothermal crystallization behaviors were investigated through the analysis of the crystallization process parameters: the nonisothermal crystallization kinetic parameters determined by the Jeziorny and Ozawa methods and the crystallization activation energy evaluated by the Kissinger method. The influence of the cooling rate and the SF content on the nonisothermal crystallization behaviors of the SF/PCL composites was examined.

## EXPERIMENTAL

### Materials

PCL in this study was a commercial product of Solvay Group (Brussels, Belgium) with a number-average molecular weight of $9.0 \times 10^4$ g/mol. The silk fiber, spun from the cocoons of *B. mori*, was supplied by JinLi Silk Co., Ltd. (Yuhang, China). Before use, the continuous silk fiber was first chopped into short fibers with an approximate length of 1.5 cm in the laboratory, degummed by boiling in a 0.5 wt % $Na_2CO_3$ water solution for 40 min to remove the sericin, and then rinsed in deionized water and dried *in vacuo* at 70°C for 2 days.

### Composite preparation

SF/PCL composites were prepared by the melt blending of PCL and SF in a Haake Rheocord 900 rheometer (Haake Mess-Technic GmbH, Karlsruhe, Germany) at 140°C with a constant screw rotation speed of 100 rpm for 15 min until the equilibrium torque was reached, and then the obtained composites were hot-pressed into thin sheets at 140°C. With fiber contents of 15, 25, 35, 45, and 55 wt %, these composites were designated 15SP, 25SP, 35SP, 45SP, and 55SP respectively.

### Crystalline structure characterization

Wide-angle X-ray diffraction patterns were obtained at room temperature from a D8 Advance automatic powder diffractometer (Bruker, Bremen, Germany) equipped with Ni-filtered Cu Kα radiation (Cu $K\alpha_1$ = 0.15406 nm) in the reflection mode. The diffractometer parameters were a divergence slit of 1°, a receiving slit of 0.2 mm, and a scatter slit of 1°. All the measurements were operated at 40 kV and 40 mA from 1 to 50° with a 2θ scanning rate of 2°C/min.

### Morphology observation

An S-2150 scanning electron microscope (Hitachi, Ltd., Tokyo, Japan) was used for morphology observation of SF/PCL composites. Before scanning electron microscopy observation, the test specimens of SF/PCL composites were first cold-fractured in liquid nitrogen, and then the fractured cross sections of these specimens were coated with a thin layer of gold.

### Nonisothermal crystallization operation

In a Q10 system (TA Instrument, New Castle, DE) calibrated with an indium standard in an atmosphere of nitrogen, samples with a weight of about 10 mg were quickly heated to 90°C, held there for 5 min to eliminate the previous thermal history, cooled at different rates (2.5, 5, 10, 20, and 30°C/min), and then heated again to 90°C at 10°C/min. The change in the heat capacity with temperature was monitored during cooling scans. The crystallization peak temperature ($T_c$) and the values of the crystallization enthalpy ($\Delta H_c$) from the first cooling scan were determined from the exothermic peak values and the exothermic peak areas. The melting peak temperature ($T_m$) from the second heating scan was determined from the endothermic peak values. The normalized crystallization enthalpy ($\Delta H_c/\chi$) was defined to test the actual effect of the fiber on the crystallization of the PCL phase in SF/PCL composites; $\chi$ is the weight ratio of PCL in SF/PCL composites.

## RESULTS AND DISCUSSION

### Crystalline structure analysis

Figure 1 presents the X-ray reflection patterns of SF, PCL, and SF/PCL composites. SF exhibits no

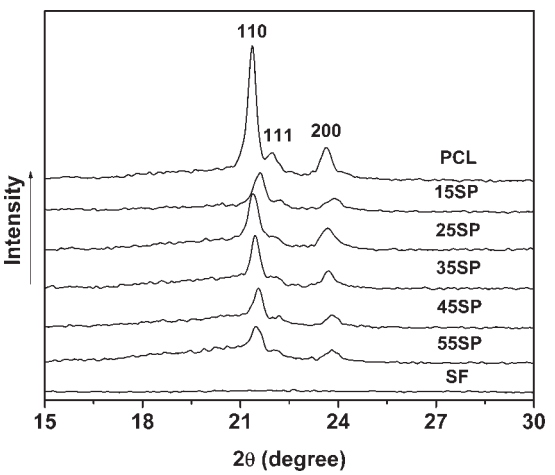


**Figure 1** Wide-angle X-ray diffraction patterns of SF, PCL, and SF/PCL composites.

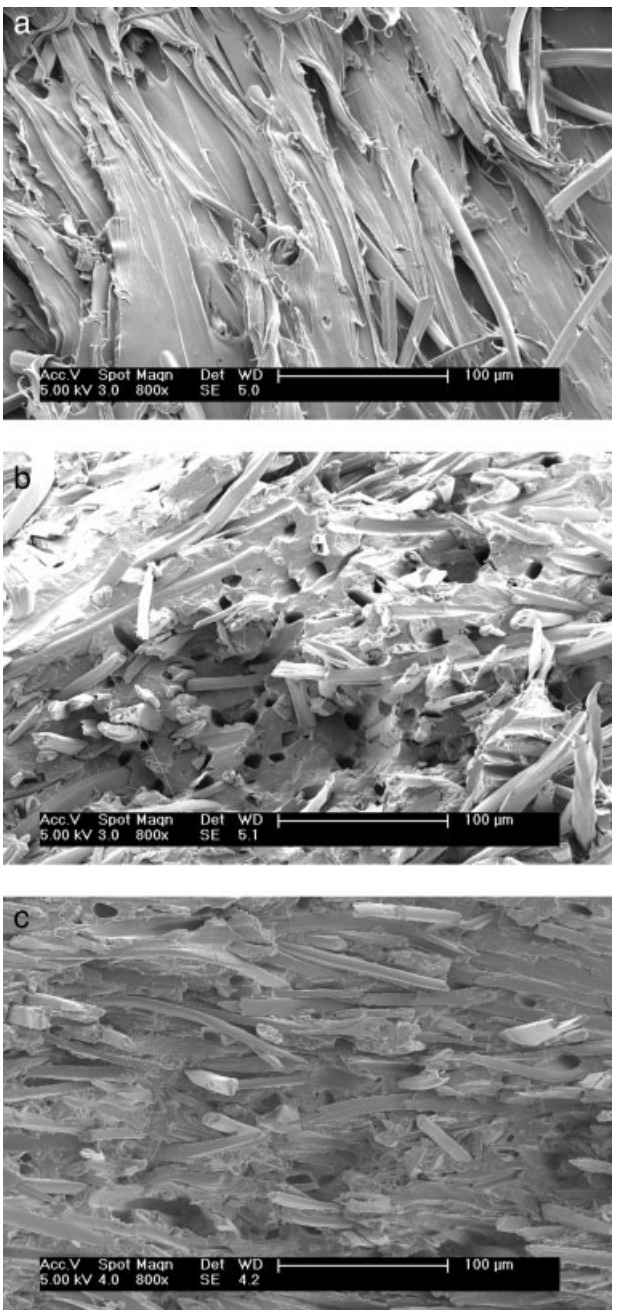


**Figure 2** Scanning electron microscopy photographs of the fractured surfaces of SF/PCL composites: (a) 25SP, (b) 35SP, and (c) 45SP.

obvious diffraction peak, whereas PCL and all the SF/PCL composites exhibit three pronounced diffraction peaks between 21 and 24° corresponding to the diffraction of crystalline planes of (110), (111), and (200) in PCL.[24,26,27] After the introduction of SF, the characteristic reflection peaks of PCL obviously shift to a higher diffraction angle and become weaker and broader. This phenomenon becomes more remarkable with an increase in the fiber content, especially in the (110) crystalline plane. It is apparent that the degree of crystallinity of PCL decreases in these SF/PCL hybrid systems, but the crystalline structure of PCL is not changed with the filling of SF.

### Morphology observation

The scanning electron micrographs of the fractured surfaces of the SF/PCL composites are shown in Figure 2. The rigid, rodlike SF is uniformly dispersed in the PCL matrix. With the fiber content increasing, the continuous PCL phase becomes unclear, and the rigid fiber network structures become more apparent. This phenomenon implies that after the construction of rigid fiber network structures, the mobility of PCL molecular chains is restricted by the confinement of the fiber network, just as reflected by the change in the X-ray diffraction peaks and crystallite size of PCL in the SF/PCL composites.

### Crystallization process analysis

According to previous research work,[28] the pure silk fibroin shows an exothermic peak and an

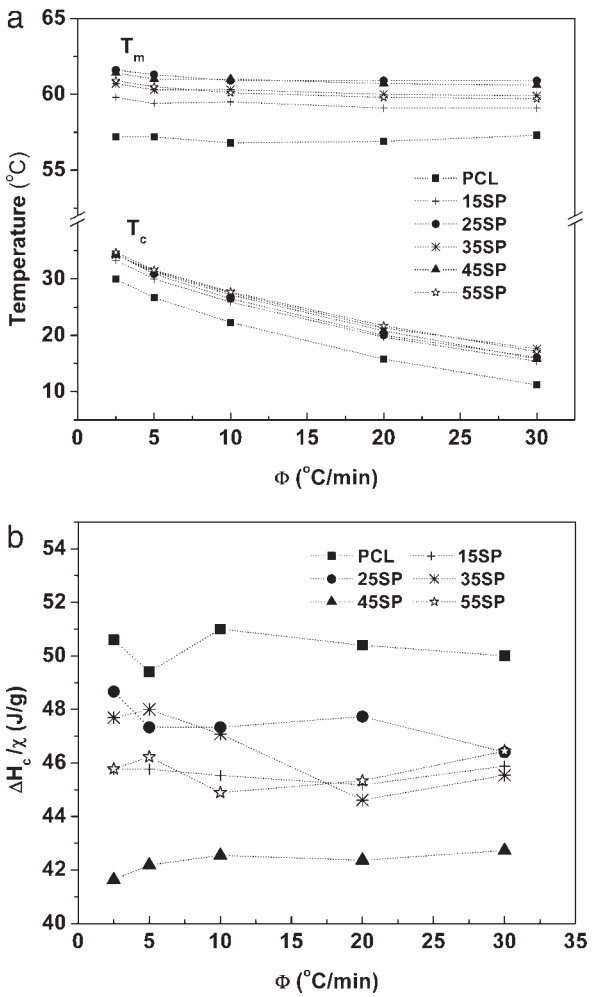


**Figure 3** $T_c$, $\Delta H_c/\chi$, and $T_m$ from the first cooling scan and second heating scan for PCL and SF/PCL composites: (a) $T_c$ and $T_m$ versus Φ and (b) $\Delta H_c/\chi$ versus Φ.

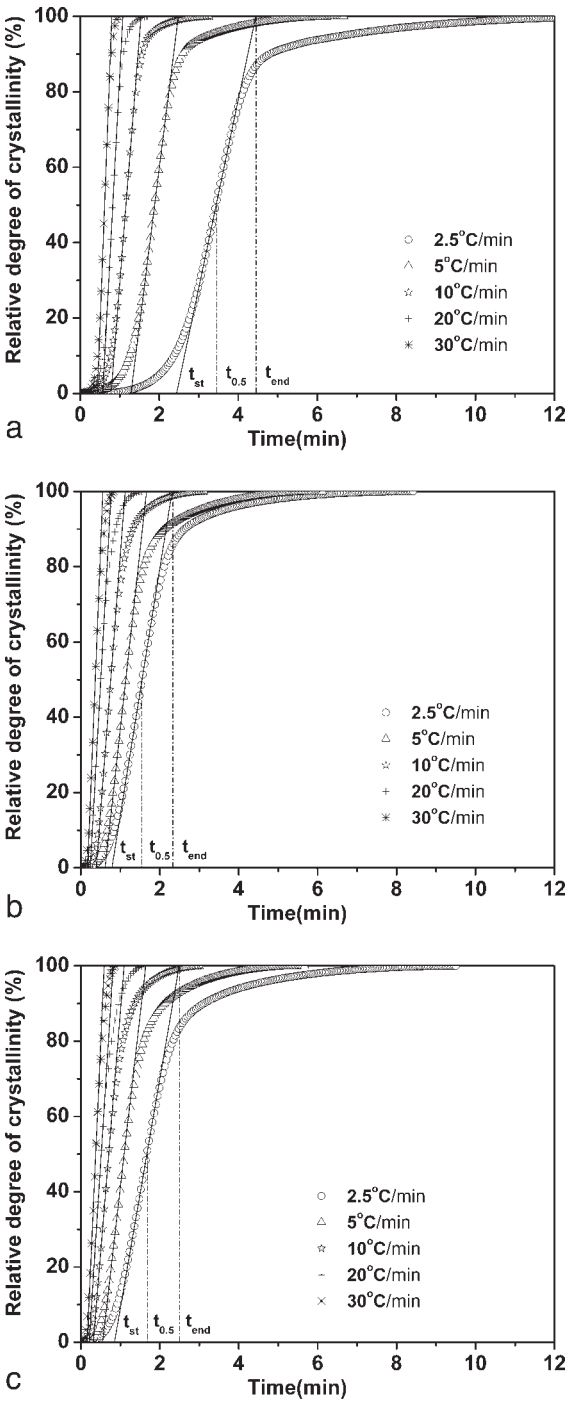


**Figure 4** Plots of $X_t$ versus time for PCL and SF/PCL composites: (a) PCL, (b) 25SP, and (c) 45SP.

endothermic peak around 220 and 280°C, respectively, during differential scanning calorimetry scans, which originate from the conformational transition of silk fibroin from a random coil to a β-sheet structure and the thermal decomposition of silk fibroin separately. Therefore, in our study, the melting and crystallization behaviors of SF/PCL composites from −10 to 90°C are merely related to the behaviors of PCL. The resultant $T_c$, $\Delta H_c/\chi$, and $T_m$ values from the cooling scan at different rates and the second heating scan at 10°C/min are shown in Figure 3 for PCL and SF/PCL composites. With the cooling rate increasing, $T_c$ becomes lower, $\Delta H_c/\chi$ is nearly unchanged, and $T_m$ decreases slightly. With an elevated SF content, $T_c$ and $T_m$ become higher, whereas $\Delta H_c/\chi$ decreases obviously. A higher cooling rate means more energy provided to get a shorter crystallization period, thus helping to increase the supercooling degree and

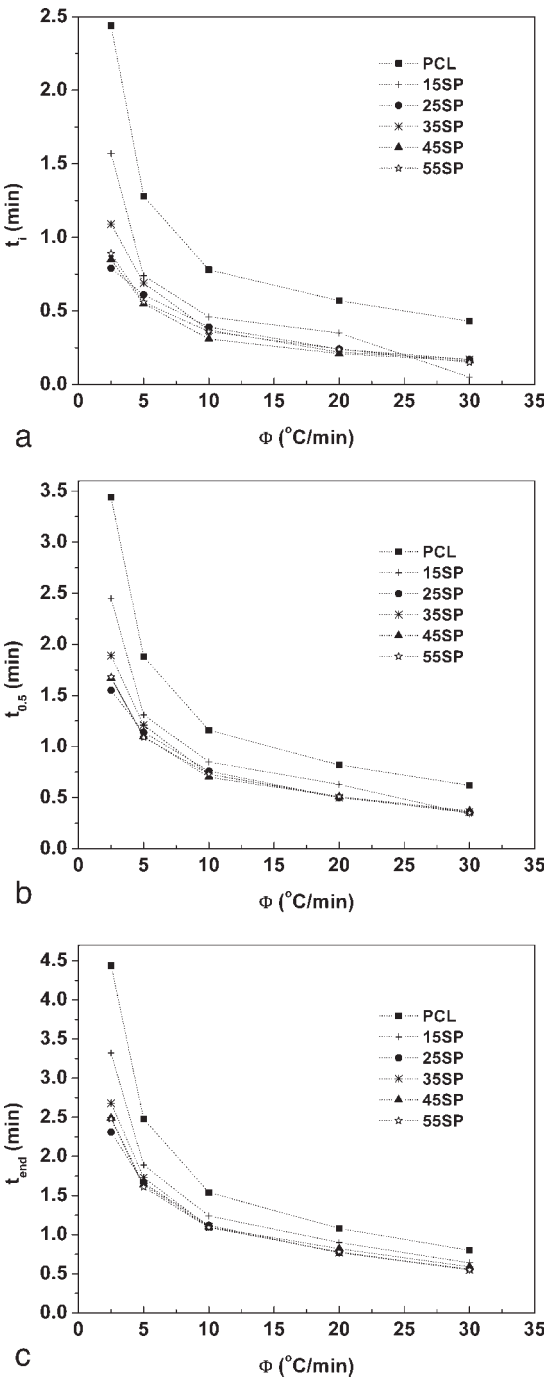


**Figure 5** Relationship of the characteristic crystallization time and Φ for PCL and SF/PCL composites: (a) $t_i$ versus Φ, (b) $t_{0.5}$ versus Φ, and (c) $t_{end}$ versus Φ.

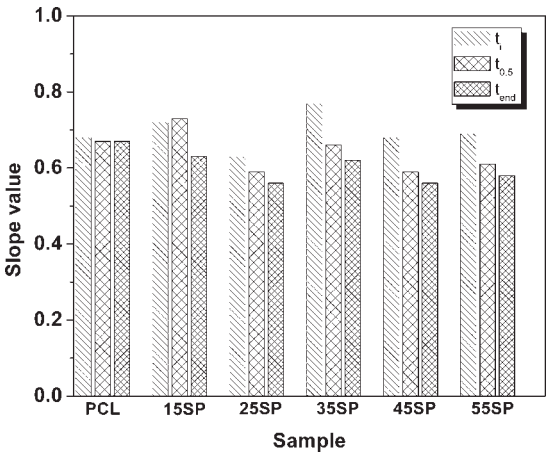


**Figure 6** Slopes of the linear relationship of plots of ln $t$ versus ln $\Phi$ for PCL and SF/PCL composites.

leading to a lower $T_c$ value and quicker crystallization. However, the crystallization exothermicity of PCL does not change with the cooling rate obviously. After the introduction of SF, the heterogeneous nucleation reagent effect of the fiber filler accelerates the primary crystallization of PCL, with $T_c$ increasing and the supercooling degree correspondingly decreasing during the crystallization process. On the other hand, with the gradual addition of the fiber filler, the construction of fiber network structures confines the mobility of PCL molecular chains and causes the corresponding decrease in the crystallization exothermicity.

The relative degree of crystallinity ($X_t$) as a function of the crystallization temperature can be determined by the ratio of the area of the exothermic peak at crystallization time $t$ to the total area of the exothermic peak:

$$X_t = \frac{\int_0^t (\frac{dH_c}{dt})dt}{\int_0^\infty (\frac{dH_c}{dt})dt} \quad (1)$$

where $dH_c$ represents the crystallization enthalpy change at time $t$, $t = 0$ represents the time at the moment of attainment of thermal equilibrium, and $t = \infty$ represents the time at the end of crystallization. According to the relation, $t = (T_0 - T)/\Phi$, where $T_0$ is the initial crystallization temperature, $T$ is the temperature at $t$, $\Phi$ is the cooling rate, and the dependence of $X_t$ on $T$ can be easily converted to the dependence of $X_t$ on $t$. Plots of $X_t$ against $t$ for each cooling rate of PCL and 25SP are given in Figure 4, where 25SP and 45SP are provided as representatives for the SF/PCL composites because of the similar shapes that their plots exhibit. It can be observed from Figure 4 that $X_t$ increases with increasing time. With the cooling rate and fiber content rising, the sigmoid curve shifts left and becomes steeper and steeper with an obviously shortened time range for crystallization, indicating the controlling role of nucleation.

The crystallization process of a supercooled molten polymer usually experiences the processes of slow crystallization at the beginning, accelerated crystallization after the incubation period, retarded crystallization after the maximum crystallization rate, and again slow crystallization tending toward equilibrium at the end. When a tangent is drawn on the

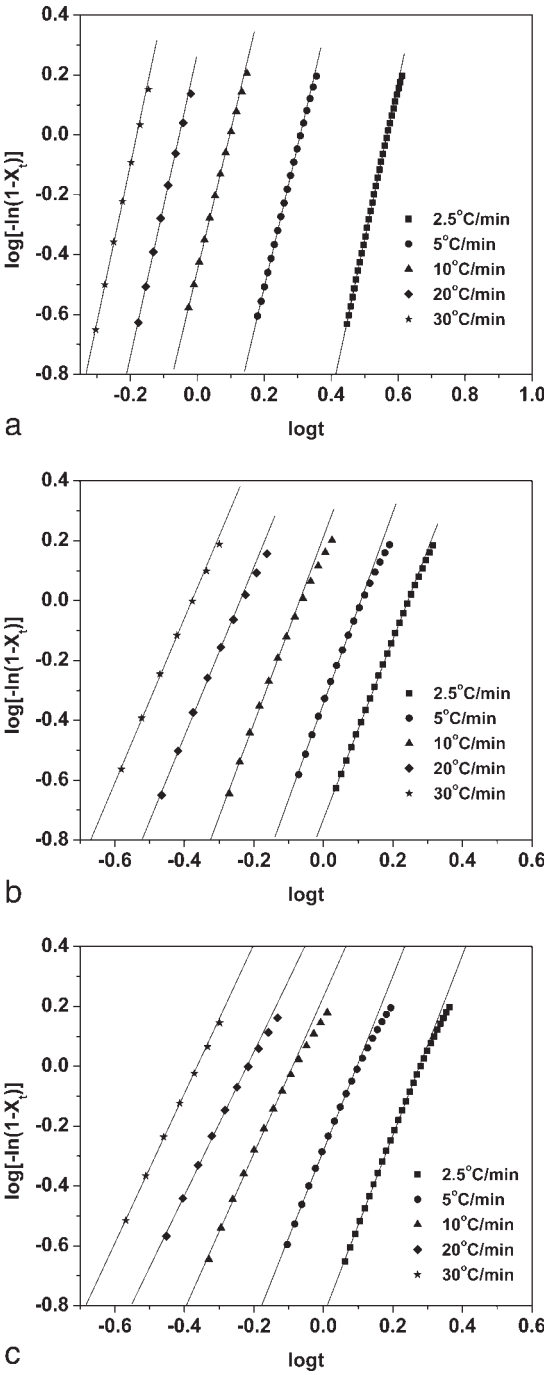


**Figure 7** Plots of log[$-\ln(1 - X_t)$] versus log $t$ for PCL and SF/PCL composites at different cooling rates: (a) PCL, (b) 25SP, and (c) 45SP.

**TABLE I**
**Kinetic Parameters Evaluated by the Jeziorny Method for PCL and SF/PCL Composites**

| | Φ | $Z_t$ | $Z_c$ | $t_{max}$ | $K_{max}$ | $G$ | $G_c$ |
|---|---|---|---|---|---|---|---|
| PCL | 2.5 | $1.08 \times 10^{-3}$ | $6.51 \times 10^{-2}$ | 3.54 | 0.35 | 1.45 | 0.58 |
| | 5 | $3.49 \times 10^{-2}$ | 0.51 | 1.93 | 0.62 | 3.22 | 0.64 |
| | 10 | 0.35 | 0.90 | 1.19 | 1.01 | 6.82 | 0.68 |
| | 20 | 1.87 | 1.03 | 0.85 | 1.45 | 13.72 | 0.69 |
| | 30 | 8.97 | 1.08 | 0.63 | 1.97 | 21.16 | 0.71 |
| 15SP | 2.5 | $1.58 \times 10^{-2}$ | 0.19 | 2.51 | 0.46 | 1.77 | 0.71 |
| | 5 | 0.27 | 0.77 | 1.32 | 0.78 | 4.02 | 0.80 |
| | 10 | 1.19 | 1.02 | 0.85 | 1.18 | 8.56 | 0.86 |
| | 20 | 3.50 | 1.06 | 0.63 | 1.64 | 17.07 | 0.85 |
| | 30 | 11.65 | 1.09 | 0.38 | 2.48 | 28.85 | 0.96 |
| 25SP | 2.5 | 0.19 | 0.51 | 1.53 | 0.62 | 2.10 | 0.84 |
| | 5 | 0.45 | 0.85 | 1.14 | 0.87 | 3.99 | 0.80 |
| | 10 | 1.63 | 1.05 | 0.75 | 1.29 | 8.59 | 0.86 |
| | 20 | 4.77 | 1.08 | 0.49 | 1.84 | 18.52 | 0.93 |
| | 30 | 10.97 | 1.08 | 0.35 | 2.51 | 29.10 | 0.97 |
| 35SP | 2.5 | $7.29 \times 10^{-2}$ | 0.35 | 1.91 | 0.55 | 1.97 | 0.79 |
| | 5 | 0.35 | 0.81 | 1.23 | 0.85 | 3.89 | 0.78 |
| | 10 | 1.71 | 1.05 | 0.73 | 1.29 | 8.51 | 0.85 |
| | 20 | 4.52 | 1.08 | 0.48 | 1.82 | 18.30 | 0.92 |
| | 30 | 11.90 | 1.09 | 0.35 | 2.57 | 29.82 | 0.99 |
| 45SP | 2.5 | 0.15 | 0.46 | 1.65 | 0.57 | 2.09 | 0.83 |
| | 5 | 0.52 | 0.88 | 1.08 | 0.86 | 4.16 | 0.83 |
| | 10 | 1.70 | 1.05 | 0.68 | 1.26 | 8.83 | 0.88 |
| | 20 | 3.37 | 1.06 | 0.48 | 1.65 | 18.30 | 0.92 |
| | 30 | 8.07 | 1.07 | 0.35 | 2.33 | 29.84 | 0.99 |
| 55SP | 2.5 | 0.13 | 0.45 | 1.68 | 0.58 | 2.12 | 0.85 |
| | 5 | 0.53 | 0.88 | 1.08 | 0.89 | 4.20 | 0.84 |
| | 10 | 1.75 | 1.06 | 0.72 | 1.30 | 8.82 | 0.88 |
| | 20 | 4.34 | 1.08 | 0.50 | 1.79 | 18.61 | 0.93 |
| | 30 | 10.19 | 1.08 | 0.33 | 2.53 | 30.89 | 1.03 |

curves in Figure 4, the points obtained from the intersection of the tangent and the lines $X_t = 100\%$ and $X_t = 0$ correspond to the start crystallization time [incubation period ($t_i$)] and the end crystallization time ($t_{end}$). The half-crystallization time ($t_{0.5}$) can also be evaluated from the time for the crystallization extent of 50%. The characteristic time parameters ($t_i$, $t_{0.5}$, and $t_{end}$) are shown as a function of the cooling rate in Figure 5. At a higher cooling rate, the characteristic crystallization time becomes shorter. A higher cooling rate corresponds to a greater supercooling degree and more energy provided for crystallization, thus shortening the crystallization time. After the addition of fiber, the characteristic crystallization time is remarkably reduced for each cooling rate. This phenomenon should be attributed to the heterogeneous nucleation reagent effect of the fiber filler in these hybrid materials. The double-logarithm plots of the cooling rate versus the characteristic time of PCL and SF/PCL composites show very good linear relationships, and the corresponding slope values of these linear relationships are shown in Figure 6. In Figure 6, for PCL, all three ln $t$–ln Φ curves are parallel with the same slope of 0.67, whereas for SF/PCL composites, the slope of the ln $t$–ln Φ curve decreases from $t_i$ to $t_{0.5}$ to $t_{end}$ in turn. Thus, the cooling rate exhibits the same influence on $t_i$, $t_{0.5}$, and $t_{end}$ for PCL but a greater influence on $t_i$ than on $t_{0.5}$ and $t_{end}$ for SF/PCL composites, and this indicates that the fiber filler has a great influence on the primary crystallization of PCL.

### Jeziorny method analysis

On the basis of the assumption of infinitesimal isothermal crystallization and Ziabacki theory, Jeziorny[29] extended the Avrami equation and described the nonisothermal crystallization kinetics as follows:

$$\log[-\ln(1 - X_t)] = \log Z_t + n \log t \tag{2}$$

$$t_{max} = \left[\frac{(n-1)}{nZ_t}\right]^{1/n} \tag{3}$$

$$G = (\pi/\ln 2)^{1/2} K_{max} D/2 \tag{4}$$

$$\log Z_c = \log Z_t/\Phi \tag{5}$$

$$G_c = G/\Phi \tag{6}$$

where $X_t$ is the degree of crystallization transformation, $Z_t$ is the composite crystallization rate constant, $n$ is the Avrami exponent, $t_{max}$ represents the time at

which the maximum crystallization rate is reached, $G$ is the kinetic crystallizability, $K_{max}$ is the rate constant corresponding to maximum crystallization, and $D$ is the half-width of the crystallization curve. With an assumption of a constant cooling rate and adequate correction of $Z_t$ and $G$ by the cooling rate factor, $Z_c$ and $G_c$ can be obtained to characterize the nonisothermal crystallization kinetics. All these kinetic parameters can be determined by the intercepts and slopes of the plots of $\log[-\ln(1 - X_t)]$ versus $\log t$ and the related equations.

Plots of $\log[-\ln(1 - X_t)]$ versus $\log t$ of PCL and SF/PCL composites are shown in Figure 7, where 25SP and 45SP are representatives for the SF/PCL composites because of the similarity of their plots. These curves exhibit a good linear relationship for PCL. However, for SF/PCL composites, some deviations from the linear relationship appear in the later stage of crystallization and appear earlier with the increase in the cooling rate and SF content. In common, the deviation originates from secondary crystallization. At a higher cooling rate and a greater SF content, the higher degree of supercooling and stronger nucleation reagent effect of the fiber filler result in a rapid arrangement of molecular chains and high imperfection and nonstabilization of crystals, thus causing the earlier appearance of the secondary crystallization. As for the same cooling rate of 5.0°C/min, the deviation of 15SP occurs at about $X_t = 75\%$, whereas the deviation of 55SP occurs at about $X_t = 70\%$. From the linear part of the plots of $\log[-\ln(1 - X_t)]$ versus $\log t$, nonisothermal crystallization kinetic parameters of PCL and SF/PCL composites have been obtained, and they are listed in Table I.

Just as shown in Table I, PCL and SF/PCL composites show a similar change tendency, $Z_c$, $K_{max}$, and $G_c$ becoming larger and $t_{max}$ becoming shorter with an increase in the cooling rate. In addition, with the cooling rate rising, the change extent of $Z_c$, $t_{max}$, and $G_c$ becomes smaller, but that of $K_{max}$ becomes greater gradually. A higher cooling rate helps to crystallize quickly and promotes the crystallization rate constant and kinetic crystallizability. After the introduction of SF, the crystallization rate constant and kinetic crystallizability of PCL are further enhanced, and this should be attributed to the heterogeneous nucleation reagent effect of the fiber filler, in good agreement with the results in Figure 5. However, the SF content does not influence the crystallization rate constant and kinetic crystallizability of SF/PCL composites very much.

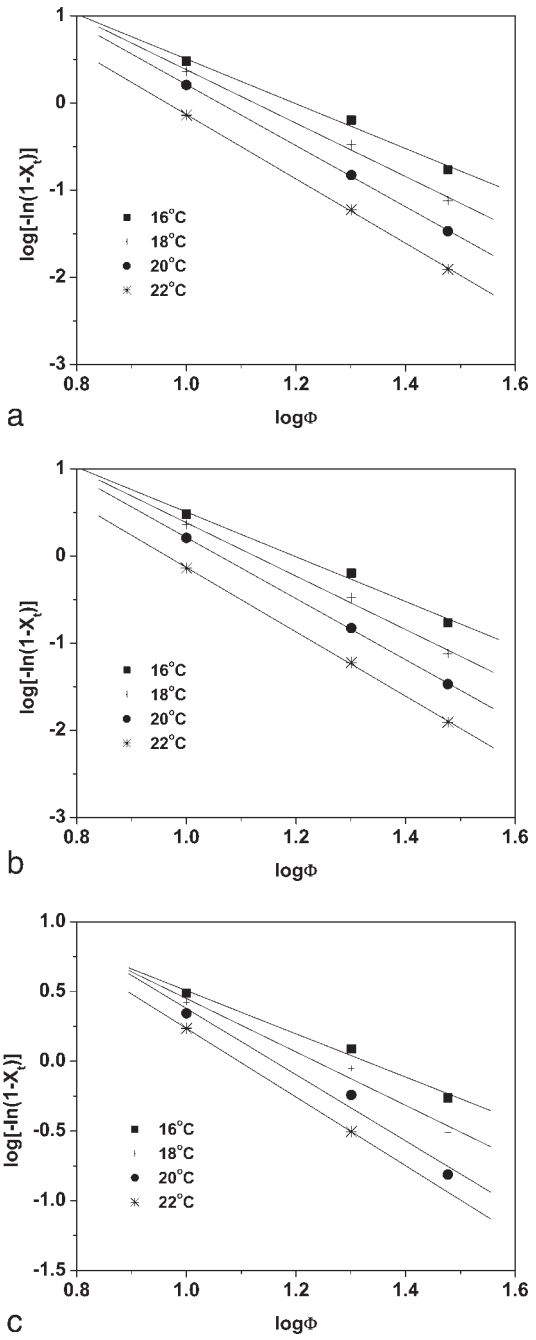


**Figure 8** Plots of $\log[-\ln(1 - X_t)]$ versus $\log \Phi$ for PCL and SF/PCL composites at different $T_c$ values: (a) PCL, (b) 25SP, and (c) 45SP.

## Ozawa method description

Ozawa analysis is a modification of the Avrami equation that replaces $t$ with $T/\Phi$ to evaluate the influence of the cooling rate on the crystallization of the polymer melt. It can be expressed by the following equation with a double-logarithm form:

$$\log[-\ln(1 - X_t)] = \log K(T) - m \log \Phi \qquad (7)$$

where $X_t$ is the degree of conversion at temperature $T$; $K(T)$ is the cooling function of temperature that is relevant to the nucleus formation, nucleation rate, and nucleus growth rate; and $m$ is the Ozawa exponent dependent on the dimension of crystal

**TABLE II**
**Kinetic Parameters Evaluated by the Ozawa Method for PCL and SF/PCL Composites**

| | | PCL | 15SP | 25SP | 35SP | 45SP | 55SP |
|---|---|---|---|---|---|---|---|
| 16°C | $m$ | 2.57 | 1.61 | 1.28 | 1.48 | 1.55 | 1.48 |
| | $K(T)$ | 1180.32 | 142.92 | 66.10 | 109.19 | 113.71 | 116.09 |
| 18°C | $m$ | 3.06 | 2.04 | 1.62 | 1.85 | 1.91 | 1.82 |
| | $K(T)$ | 2795.12 | 331.51 | 130.86 | 223.77 | 230.04 | 223.20 |
| 20°C | $m$ | 3.50 | 2.61 | 2.09 | 2.44 | 2.37 | 2.30 |
| | $K(T)$ | 5205.95 | 1030.86 | 321.66 | 761.38 | 562.86 | 564.81 |
| 22°C | $m$ | 3.69 | 2.79 | 2.74 | 2.46 | 2.46 | 2.33 |
| | $K(T)$ | 3628.27 | 1037.29 | 1188.78 | 573.72 | 498.36 | 441.47 |

growth.[30] By the selection of a certain temperature, the data of the degree of conversion at various cooling rates can be obtained; plots of $\log[-\ln(1 - X_t)]$ versus $\log \Phi$ of PCL and SF/PCL composites are drawn in Figure 8, where 25SP and 45SP are representatives for the SF/PCL composites because of the similarity of their plots. From the intercepts and slopes of the linear relationship of the plots of $\log[-\ln(1 - X_t)]$ versus $\log \Phi$, $K(T)$ and $m$ can be determined, as shown in Table II.

As shown in Figure 8, the temperatures of 16, 18, 20, and 22°C were selected, and the resultant points show a quite good linear relationship but different slopes with different temperatures. From Table II, it can be found that $m$ is not constant, and with the temperature rising, both $m$ and $K(T)$ increase; this is quite different from the results of PCL/$SiO_2$ hybrid materials with a continuous decrease in $m$ and $K(T)$.[24] Thus, it can be seen that the filler addition (SF or $SiO_2$) does cause various nucleation and growth mechanisms of the crystalline phase with different temperatures during the nonisothermal crystallization process. The addition of different fibers also shows different effects on the crystallization mechanism. Moreover, $m$ of PCL is above 2, whereas $m$ of SF/PCL composites is less than 2; this also verifies that heterogeneous nucleation is dominant in the nonisothermal crystallization process of PCL in SF/PCL composites.[31]

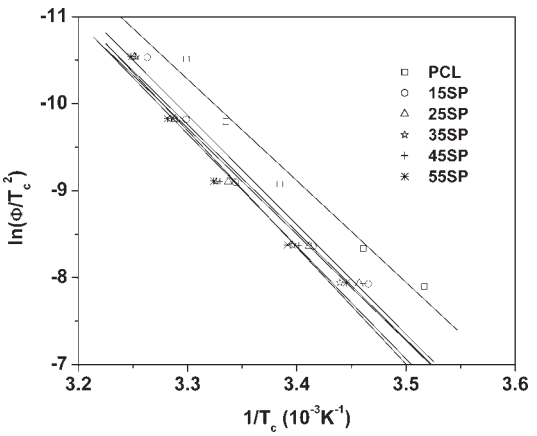


**Figure 9** Plot of $\ln(\Phi/T_c^2)$ versus $1/T_c$ for PCL and SF/PCL composites.

### Determination of the crystallization activation energy

In general, the nonisothermal melt crystallization peak temperature shifts to a lower temperature range with the cooling rate increasing. This change tendency in differential thermal analysis can be used to further investigate the crystallizability of PCL and SF/PCL composites, just as described in the Kissinger method.[32] The Kissinger equation can be written as follows:

$$d\ln(\Phi/T_c^2)/d(1/T_c) = -\Delta E/R \quad (8)$$

where $\Delta E$ is the crystallization activation energy, $R$ is the universal gas constant, and the value of $\Delta E$ can be obtained from the slope of the plot of $\ln(\Phi/T_c^2)$ versus $1/T_c$ (Fig. 9). The values of $\Delta E$ were found to be 97.13, 104.67, 102.67, 111.53, 101.52, and 107.52 kJ/mol for PCL, 15SP, 25SP, 35SP, 45SP, and 55SP, respectively. $\Delta E$ is the activation energy required to transport molecular chains to the crystallization surface. The addition of SF slightly increases the energy barrier, and this indicates the weakening of the transportation ability of molecular chains with the confinement environment of the fiber network structure.

## CONCLUSIONS

As the cooling rate increases, the crystallization of PCL and SF/PCL composites exhibits a similar change tendency, such as a decrease in $T_c$, an inconspicuous change in $\Delta H_c/\chi$, and a shortening of the crystallization time. With an increase in the SF content, the strengthening of the heterogeneous nucleation reagent effect leads to the rising of $T_c$ and the acceleration of the crystallization process for PCL. Unlike the crystallization behavior of PCL, secondary crystallization behavior occurs for the SF/PCL composites and becomes more and more remarkable with increases in the cooling rate and SF

content. Moreover, with the introduction of SF and the increase in the cooling rate, the nucleation and growth mode of the PCL crystalline phase is slightly changed during the nonisothermal crystallization process. Because of the confinement environment of the fiber network structure, the transportation ability of PCL molecular chains is weakened, the crystallite size of PCL is reduced, and the crystallization activation energy increases.

The authors thank the Instrumental Analysis Center of Shanghai Jiao Tong University for its assistance with the measurements.

## References

1. Zhou, S.; Deng, X.; Yang, H. Biomaterials 2003, 24, 3563.
2. Ciapetti, G.; Ambrosio, L.; Savarino, L.; Granchi, D.; Cenni, E.; Baldini, N.; Pagani, S.; Guizzardi, S.; Causa, F.; Giunti, A. Biomaterials 2003, 24, 3815.
3. Mishra, S.; Mohanty, A. K.; Drzal, L. T.; Misra, M.; Parija, S.; Nayak, S. K.; Tripathy, S. S. Compos Sci Technol 2003, 63, 1377.
4. Cyras, V. P.; Kenny, J. M.; Vázquez, A. Polym Eng Sci 2001, 41, 1521.
5. Funabashi, M.; Kunioka, M. Green Chem 2003, 5, 591.
6. Teramoto, N.; Urata, K.; Ozawa, K. Polym Degrad Stab 2004, 86, 401.
7. Yang, A.; Wu, R. J Appl Polym Sci 2002, 84, 486.
8. Chen, B. Q.; Sun, K.; Ren, T. Eur Polym J 2005, 41, 453.
9. Nitz, H.; Semke, H.; Landers, R.; Mulhaupt, R. J Appl Polym Sci 2001, 81, 1972.
10. Ruseckaite, R. A.; Jimenez, A. Polym Degrad Stab 2003, 81, 353.
11. Shao, Z.; Vollrath, F. Nature 2002, 418, 741.
12. Freddi, G.; Mossotti, R.; Innocenti, R. J Biotechnol 2003, 106, 101.
13. Pérez-Rigueiro, J.; Elices, M.; Llorca, J.; Viney, C. J Appl Polym Sci 2002, 84, 1431.
14. Pérez-Rigueiro, J.; Viney, C.; Llorca, J.; Elices, M. J Appl Polym Sci 1998, 70, 2439.
15. Lee, S. M.; Cho, D.; Park, W. H.; Lee, S. G.; Han, S. O.; Drzal, L. T. Compos Sci Technol 2005, 65, 647.
16. Addonizio, M. L.; Martuscelli, E.; Silvestre, C. Polymer 1987, 28, 183.
17. Liu, T. X.; Mo, Z. S.; Zhang, H. F. J Appl Polym Sci 1998, 67, 815.
18. An, Y. X.; Liu, T. X.; Dong, L. S.; Mo, Z. S.; Feng, Z. L. J Polym Sci Part B: Polym Phys 1998, 36, 1305.
19. Liu, S. Y.; Yu, Y. N.; Cui, Y.; Zhang, H. F.; Mo, Z. S. J Appl Polym Sci 1998, 70, 2371.
20. Avrami, M. J Chem Phys 1939, 7, 1103.
21. Avrami, M. J Chem Phys 1940, 8, 212.
22. Wu, T. M.; Chen, E. C. Polym Eng Sci 2006, 46, 1309.
23. Nie, K. M.; Pang, W. M.; Zheng, S. X.; Wang, Y. S.; Lu, F.; Zhu, Q. R. Polym Int 2005, 54, 327.
24. Jiang, S. C.; Ji, X. L.; An, L. J.; Jiang, B. Z. Polymer 2001, 42, 3901.
25. Homminga, D.; Goderis, B.; Dolbnya, I.; Groeninckx, G. Polymer 2006, 47, 1620.
26. Wu, T. M.; Chen, E. C. J Polym Sci Part B: Polym Phys 2006, 44, 598.
27. Alexander, L. E. X-Ray Diffraction Methods in Polymer Science; Wiley-Interscience: New York, 1969.
28. Lee, K. H. Macromol Rapid Commun 2004, 25, 1792.
29. Jeziorny, A. Polymer 1978, 19, 1142.
30. Ozawa, T. Polymer 1971, 12, 150.
31. Zhu, G. M.; Xu, Q. Y.; Qin, R. F.; Yan, H. X.; Liang, G. Z. Rad Phys Chem 2005, 74, 42.
32. Kissinger, H. E. J Res Natl Bur Stand 1956, 57, 217.